

# QCD at small non-zero quark chemical potentials

J.B. Kogut and D. Toublan

*Loomis Laboratory of Physics, University of Illinois, Urbana-Champaign, IL 61801, USA*

## Abstract

We study the effects of small chemical potentials associated with the three light quark flavors in QCD. We use a low-energy effective field theory that solely relies on the symmetries of the QCD partition function. We find three different phases: a normal phase, a pion superfluid phase and a kaon superfluid phase. The two superfluid phases are separated by a first order phase transition, whereas the normal phase and either of the superfluid phases are separated by a second order phase transition. We compute the quark-antiquark condensate, the pion condensate and the kaon condensate in each phase, as well as the isospin density, the strangeness density, and the mass spectrum.

*PACS:*11.30.Rd; 12.39.Fe; 12.38.Lg; 71.30.+h

*Keywords:* QCD phase diagram; Pion condensate; Kaon condensate; Low-energy effective field theory; Chiral Perturbation Theory

## 1 Introduction

QCD at non-zero baryon density has recently been the subject of many studies. Our present knowledge of nucleon rich matter is limited to low densities and very high densities. In the first regime, we can rely on our good phenomenological understanding of nuclear interactions in the vacuum. In the second regime, the phenomenon of color superconductivity and its consequences are becoming better understood both qualitatively and quantitatively [1, 2, 3, 4]. However we have only a poor grasp of a sample of nuclear matter that is neither too dilute nor too dense. Unfortunately this kind of matter is found in many interesting physical systems, from supernova explosions and neutron stars to heavy ion collisions. In other words, our knowledge of the QCD phase diagram at non-zero chemical potential is limited to extreme cases, and it is clear that we need a better understanding of its characteristics.

This situation is very different from what we know about QCD at non-zero temperature and zero chemical potential, where numerous analytic and numerical studies have enabled us to achieve a qualitative and a quantitative understanding [5]. Unfortunately, the current numerical techniques are useless in the case of QCD with three colors and fermions in the fundamental

representation at non-zero baryon density. The complexity of the measure in the partition function is the origin of the problem. Special techniques have been developed to tackle this problem, but their reach is presently far from QCD [6]. There are however QCD-like theories at non-zero baryon density that do not have this complexity problem. Therefore they can be studied numerically with the usual techniques: QCD with two colors and fundamental fermions, and QCD with any number of colors and adjoint fermions. We now have a good understanding of these QCD-like theories from analytic and numerical studies [7, 8, 9, 10, 11, 12, 13]. QCD with three colors and two flavors of fundamental fermions at non-zero isospin density also has a real measure, and can therefore also be studied with standard numerical algorithms [14].

In this article we will study the QCD phase diagram for small chemical potentials associated to each quark flavor. At low enough energies, the single most important property of QCD is that chiral symmetry is spontaneously broken in the vacuum. It implies the existence of light bosonic degrees of freedom, and stringent constraints on the physical observables. This property has been extensively and successfully used to study QCD at low energy within an effective theory solely based on the symmetries of the QCD partition function, Chiral Perturbation Theory [15, 16]. Since the spontaneous breaking of chiral symmetry is still the most relevant property of QCD at low enough quark chemical potentials, Chiral Perturbation Theory should also enable us to explore the QCD phase diagram in this domain. This approach has been successfully used for QCD-like theories at non-zero baryon chemical potential and for QCD at non-zero isospin chemical potential [7, 8, 9, 14].

We will restrict ourselves to the three light quark flavors, for which this effective theory approach can be used. There is however an intrinsic limitation to this approach. Since only the octet of Goldstone bosons are kept as the relevant degrees of freedom, high chemical potentials where other excitations become relevant cannot be reached. A rapid glance at the hadron spectrum, and in particular the proton, the rho and the omega, shows that we will be able to explore the domain restricted by  $|\mu_u| < 300\text{MeV}$ ,  $|\mu_d| < 300\text{MeV}$ , and  $|\mu_s| < 550\text{MeV}$ .

Our study extends the analysis of QCD at low isospin chemical potential that included the up and down quark flavors only [14]. In this analysis, it was found that the pions form a condensate at high enough isospin chemical potential. Similarly, we will find that for high enough strange chemical potential, it is energetically favorable for the kaons to form a condensate. A non-trivial phase diagram emerges; there are three distinct phases: a normal phase, a pion condensation phase and a kaon condensation phase. The superfluid phases are separated from each other by a first order phase transition, whereas either of them is separated from the normal phase by a second order phase transition.

The pion and kaon condensates we will find in our study are very different from the pion and kaon condensates that emerge in a nucleon rich environment [17]. In this latter case, the condensation is driven by the attractive meson-nucleon interactions. In our case the baryon density is zero, and the pion and kaon condensates emerge out of the vacuum as soon as it becomes energetically favorable for the system to form such condensates in the ground state, just because of the charge carried by these modes.

We proceed as follow. First we shortly derive the effective Lagrangian in Section 2, and then determine the ground state of the effective theory in Section 3. Section 4 is devoted to the computation of the various condensates relevant to the three different phases as well as the isospin and strangeness densities. The mass spectrum is computed in Section 5. Concluding remarks and discussion are presented in the Section 6.

## 2 Low-energy Effective Lagrangian

In order to construct the low-energy effective Lagrangian, we need to study the symmetries of QCD. We work in Minkowski space. The fermionic part of the QCD Lagrangian at non-zero quark chemical potentials is given by

$$\mathcal{L}_{\text{QCD}} = \bar{\psi} \not{D} \psi + \bar{\psi} B_\nu \gamma_\nu \psi - \bar{\psi} \mathcal{M} \psi, \quad (1)$$

where

$$\psi = \begin{pmatrix} u \\ d \\ s \end{pmatrix}, \quad \mathcal{M} = \text{diag}(m_u, m_d, m_s), \quad (2)$$

$$\text{and } B_\nu = (-B, \vec{0}), \quad B = \text{diag}(\mu_u, \mu_d, \mu_s) = \text{diag}\left(\frac{1}{3}\mu_B + \frac{1}{2}\mu_I, \frac{1}{3}\mu_B - \frac{1}{2}\mu_I, \frac{1}{3}\mu_B - \mu_S\right). \quad (3)$$

One can either use chemical potentials associated with the quark flavors, or chemical potentials associated with baryon number,  $\mu_B$ , isospin,  $\mu_I$ , and strangeness,  $\mu_S$ . In this study, we will take  $m_u = m_d \equiv m$ . When all quark masses and chemical potentials vanish, the QCD Lagrangian is invariant under  $SU_L(3) \times SU_R(3) \times U_V(1)$ . At zero chemical potential, this symmetry is spontaneously broken to  $SU_V(3) \times U_V(1)$ . There are therefore eight Goldstone bosons in the spectrum:  $\pi^0, \pi^+, \pi^-, \eta^0, K^+, K^-, K^0$ , and  $\bar{K}^0$ . They are the relevant degrees of freedom at low energy.

The effective Lagrangian of QCD at low energies and finite quark chemical potentials in Minkowski space is given by

$$\mathcal{L}_{\text{eff}} = \frac{F^2}{4} \text{Tr} \nabla_\nu \Sigma \nabla_\nu \Sigma^\dagger + \frac{1}{2} G \text{Tr} \mathcal{M} (\Sigma + \Sigma^\dagger), \quad (4)$$

where  $\Sigma \in SU(3)$ , and  $\nabla_\nu \Sigma = \partial_\nu \Sigma - i[B_\nu, \Sigma]$ . This is the usual Chiral Perturbation Theory Lagrangian at lowest order [15, 16]. It contains only the octet of Goldstone bosons due to spontaneous chiral symmetry breaking. The chemical potential has been introduced in the same way as a regular vector source using the usual flavor gauge symmetry [16, 7]. Under a chiral rotation, the quark fields transform as  $(\psi_L, \psi_R) \rightarrow (V_L \psi_L, V_R \psi_R)$ , with  $V_{L,R} \in SU(3)_{L,R}$ , whereas  $\Sigma \rightarrow V_R \Sigma V_L^\dagger$ . For zero chemical potentials  $\Sigma$  is invariant under vector transformations and contains the octet of Goldstone bosons due to spontaneous chiral symmetry breaking:

$$\Sigma = U \bar{\Sigma} U, \quad \text{with } U = \exp(i\Phi/\sqrt{2}F), \quad (5)$$

and

$$\Phi = \begin{pmatrix} \frac{\pi^0}{\sqrt{2}} + \frac{\eta^0}{\sqrt{6}} & \pi^+ & K^+ \\ \pi^- & -\frac{\pi^0}{\sqrt{2}} + \frac{\eta^0}{\sqrt{6}} & K^0 \\ K^- & \bar{K}^0 & -\frac{2\eta^0}{\sqrt{6}} \end{pmatrix}, \quad (6)$$

with  $\bar{\Sigma} = \text{diag}(1, 1, 1)$  for  $\mu_B = \mu_I = \mu_S = 0$ . The effective Lagrangian is invariant under local chiral transformations. At zero chemical potentials, the masses of the Goldstone bosons are given by the Gell-Mann–Oakes–Renner relation:

$$\begin{aligned} m_\pi^2 &= 2Gm/F^2 \\ m_K^2 &= G(m + m_s)/F^2 \\ m_{\eta^0}^2 &= 2G(m + 2m_s)/3F^2 = (4m_K^2 - m_\pi^2)/3. \end{aligned} \quad (7)$$

The first remarkable property of the effective Lagrangian (4) is that in the  $(\mu_B, \mu_I, \mu_S)$ -basis,  $\mu_B$  completely drops out of  $\mathcal{L}_{\text{eff}}$ . This is just due to the fact that the effective Lagrangian contains only the octet of Goldstone bosons due to spontaneous chiral symmetry breaking. The use of the effective Lagrangian is therefore limited to  $|\mu_B| < 940\text{MeV}$ ,  $|\mu_I| < 770\text{MeV}$ , and  $|\mu_S| < 550\text{MeV}$ . These estimated bounds come from the masses of the proton, the rho and the omega, respectively. This means that the effective Lagrangian is only valid in the domain  $|\mu_u| < 300\text{MeV}$ ,  $|\mu_d| < 300\text{MeV}$ , and  $|\mu_s| < 550\text{MeV}$ . Therefore in this work, the baryon chemical potential will never appear explicitly, and we will work with  $\mu_I$  and  $\mu_S$ . Recall however that all our results are valid for  $|\mu_B| < 940\text{MeV}$ , and that Chiral Perturbation Theory, in its domain of validity, allows us to determine the phase diagram in the *three* quark chemical potentials. For definiteness, we will restrict ourselves to  $\mu_I, \mu_S > 0$ , the other quadrants in the  $(\mu_I, \mu_S)$ -plane are easily derived from our results.

### 3 Ground state

The ground state of the effective theory is determined by the maximum of the static part of the effective Lagrangian. Therefore  $\bar{\Sigma}$ , the maximum of

$$\mathcal{L}_{\text{stat}} = -\frac{F^2}{4}\text{Tr}[B, \bar{\Sigma}][B, \bar{\Sigma}^\dagger] + \frac{1}{2}G\text{Tr}\mathcal{M}(\bar{\Sigma} + \bar{\Sigma}^\dagger), \quad (8)$$

determines the ground state of QCD at non-zero quark chemical potentials.

We will use the following Ansatz for the saddle point:

$$\bar{\Sigma} = \begin{pmatrix} 1 & 0 & 0 \\ 0 & \cos \beta & -\sin \beta \\ 0 & \sin \beta & \cos \beta \end{pmatrix} \begin{pmatrix} \cos \alpha & \sin \alpha & 0 \\ -\sin \alpha & \cos \alpha & 0 \\ 0 & 0 & 1 \end{pmatrix} \begin{pmatrix} 1 & 0 & 0 \\ 0 & \cos \beta & \sin \beta \\ 0 & -\sin \beta & \cos \beta \end{pmatrix}, \quad (9)$$

with  $\alpha, \beta \in (0, \pi/2)$ . Notice that  $\bar{\Sigma}|_{\alpha=0} = \text{diag}(1, 1, 1)$  corresponds to the ground state at  $\mu_I = \mu_S = 0$ . Furthermore in the massless case,

$$\bar{\Sigma}|_{(\alpha=\frac{\pi}{2}, \beta=0)} = \begin{pmatrix} 0 & 1 & 0 \\ -1 & 0 & 0 \\ 0 & 0 & 1 \end{pmatrix} \quad (10)$$

is found to be the maximum when  $\mu_I > 2\mu_S$ , and

$$\bar{\Sigma}|_{(\alpha=\frac{\pi}{2}, \beta=\frac{\pi}{2})} = \begin{pmatrix} 0 & 0 & 1 \\ 0 & 1 & 0 \\ -1 & 0 & 0 \end{pmatrix} \quad (11)$$

is found to be the maximum when  $\mu_I < 2\mu_S$ . By noticing that the condensate is basically given by  $\bar{\psi}_R \bar{\Sigma} \psi_L$ , it is easy to see that (10) corresponds to a pion condensation phase, and that (11) corresponds to a kaon condensation phase. Our Ansatz corresponds to an axial rotation to go from the normal phase to either of the superfluid phases, and a vector rotation to go directly from one superfluid phase to the other. We will show that this Ansatz indeed corresponds to a local maximum of  $\mathcal{L}_{\text{stat}}$ . We will assume that it is the global maximum.

After our Ansatz (9) is introduced into (8), the static part of the effective Lagrangian becomes quite complicated

$$\mathcal{L}_{\text{stat}} = \frac{1}{32F^2} \left\{ (21\mu_I^2 + 12\mu_I\mu_S + 20\mu_S^2 + (19\mu_I^2 + 20\mu_I\mu_S + 12\mu_S^2) \cos \alpha) \sin^2(\alpha/2) \right.$$

$$-2(\mu_I - 2\mu_S)^2 \sin^4(\alpha/2) \cos(4\beta) + 2(\mu_I - 2\mu_S)(3\mu_I + 2\mu_S) \sin^2 \alpha \} \quad (12)$$

$$+ G \{ m \cos \alpha (1 + \cos^2 \beta) + m_s \cos^2 \beta + (m + m_s \cos \alpha) \sin^2 \beta \}.$$

We first maximize  $\mathcal{L}_{\text{stat}}$  with respect to  $\beta$ . Remember that we limit ourselves to the first quadrant in the  $(\mu_I, \mu_S)$ -plane:  $\mu_I, \mu_S > 0$ . We find that the maximum, for  $\alpha \neq 0$  and  $\beta \in (0, \pi/2)$ , is either at  $\beta = 0$  or at  $\beta = \pi/2$ . Therefore there are two different phases according to the value of  $\beta$ . We look for the maximum of  $\mathcal{L}_{\text{stat}}$  separately in each case.

- i)  $\beta = 0$ : The static part of the effective Lagrangian, its maximum, and the saddle point are given by

$$\mathcal{L}_{\text{stat}} = 2Gm \cos \alpha + Gm_s + \frac{F^2}{2} \mu_I^2 \sin^2 \alpha, \quad (13)$$

$$\text{with} \quad \begin{cases} \cos \alpha = 1 & \text{for } \mu_I < m_\pi \\ \cos \alpha = (m_\pi/\mu_I)^2 & \text{for } \mu_I > m_\pi, \end{cases} \quad (14)$$

$$\text{and} \quad \bar{\Sigma} = \begin{pmatrix} \cos \alpha & \sin \alpha & 0 \\ -\sin \alpha & \cos \alpha & 0 \\ 0 & 0 & 1 \end{pmatrix}. \quad (15)$$

- ii)  $\beta = \pi/2$ : The static part of the effective Lagrangian, its maximum, and the saddle point are given by

$$\mathcal{L}_{\text{stat}} = Gm + G(m + m_s) \cos \alpha + \frac{F^2}{2} (\frac{1}{2}\mu_I + \mu_S)^2 \sin^2 \alpha, \quad (16)$$

$$\text{with} \quad \begin{cases} \cos \alpha = 1 & \text{for } \frac{1}{2}\mu_I + \mu_S < m_K \\ \cos \alpha = (m_K/(\frac{1}{2}\mu_I + \mu_S))^2 & \text{for } \frac{1}{2}\mu_I + \mu_S > m_K, \end{cases} \quad (17)$$

$$\text{and} \quad \bar{\Sigma} = \begin{pmatrix} \cos \alpha & 0 & \sin \alpha \\ 0 & 1 & 0 \\ -\sin \alpha & 0 & \cos \alpha \end{pmatrix}. \quad (18)$$

Finally, in order to find the maximum of the static part of the effective Lagrangian in the whole quadrant  $\mu_I, \mu_S > 0$ , we have to compare the value of  $\mathcal{L}_{\text{stat}}$  for  $\alpha = 0$ , for  $\beta = 0$  and  $\cos \alpha = (m_\pi/\mu_I)^2$ , and for  $\beta = \pi/2$  and  $\cos \alpha = (m_K/(\frac{1}{2}\mu_I + \mu_S))^2$ . The orientation of the condensate for a given pair  $(\mu_I, \mu_S)$  is determined by the maximum of  $\mathcal{L}_{\text{stat}}$  at this point. We find three different phases:

1. **Normal phase:**  $\mu_I < m_\pi$  and  $\mu_S < m_K - \frac{1}{2}\mu_I$

$$\cos \alpha = 1, \text{ any } \beta \in (0, \pi/2) \quad (19)$$

2. **Pion condensation phase:**  $\mu_I > m_\pi$  and  $\mu_S < \left(-m_\pi^2 + \sqrt{(m_\pi^2 - \mu_I^2)^2 + 4m_K^2 \mu_I^2}\right)/2\mu_I$

$$\cos \alpha = \left(\frac{m_\pi}{\mu_I}\right)^2, \beta = 0 \quad (20)$$

3. **Kaon condensation phase:**  $\mu_S > m_K - \frac{1}{2}\mu_I$  and  $\mu_S > \left(-m_\pi^2 + \sqrt{(m_\pi^2 - \mu_I^2)^2 + 4m_K^2 \mu_I^2}\right)/2\mu_I$

$$\cos \alpha = \left(\frac{m_K}{\frac{1}{2}\mu_I + \mu_S}\right)^2, \beta = \pi/2. \quad (21)$$

The curve  $\mu_S = \left(-m_\pi^2 + \sqrt{(m_\pi^2 - \mu_I^2)^2 + 4m_K^2\mu_I^2}\right) / 2\mu_I$  is a first order phase transition curve, because the pion and kaon condensates compete on this curve. The phase diagram in the first quadrant and its obvious extension to the whole  $(\mu_I, \mu_S)$ -plane are given in Fig. 1 for  $m_\pi = 140\text{MeV}$ , and  $m_K = 500\text{MeV}$ . They are very similar to the phase diagram of QCD-like theories at finite baryon and isospin densities [9].

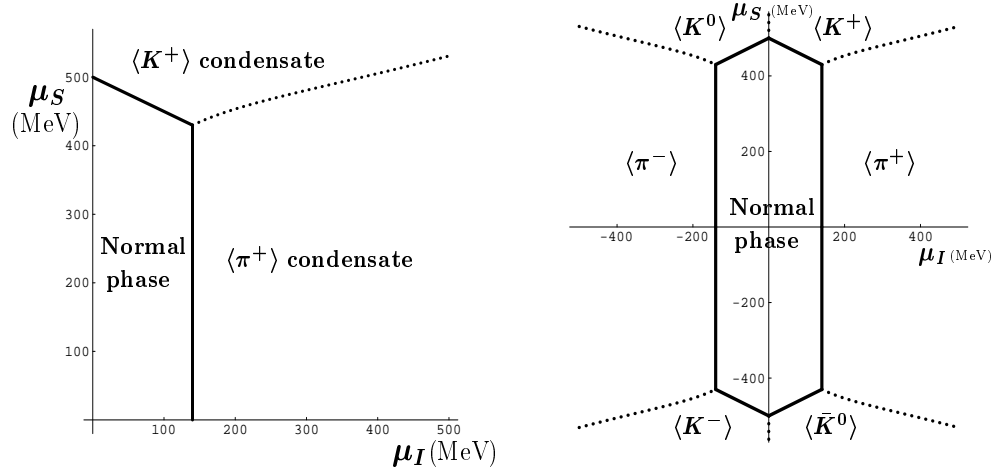


Figure 1: Phase diagram in the  $(\mu_I, \mu_S)$ -plane. The solid lines are second order phase transitions, whereas the dotted curves are first order phase transitions. The intersection of the three phase transition curves on the left figure is at  $(\mu_I, \mu_S) = (m_\pi, m_K - m_\pi/2)$ .

## 4 Condensates and charge densities

We will show in the next section that  $\bar{\Sigma}$  given by (9,19,20,21) is indeed a local maximum of the static part of the effective Lagrangian. We will assume that it is the global maximum. But first we investigate the properties of the ground state described by (9,19,20,21) in the three phases by looking at different observables. The quark-antiquark condensates,  $\langle \bar{q}q \rangle$  for  $q = u, d, s$ , the pion condensate,  $\langle \bar{d}\gamma_5 u + \text{h.c.} \rangle$ , the kaon condensate,  $\langle \bar{s}\gamma_5 u + \text{h.c.} \rangle$  are obtained by inserting the appropriate sources into the effective Lagrangian [8], or more directly by noticing that the vacuum expectation value of an operator bilinear in the quark fields is basically given by  $\langle \bar{\psi}_R \bar{\Sigma} \psi_L \rangle$  (10,11). The isospin density,  $n_I = \partial \mathcal{L}_{\text{eff}} / \partial \mu_I$ , and the strangeness density,  $n_S = \partial \mathcal{L}_{\text{eff}} / \partial \mu_S$  are easily obtained from the static part of the effective Lagrangian.

1. **Normal phase**,  $\mu_I < m_\pi$  and  $\mu_S < m_K - \frac{1}{2}\mu_I$ :

$$\begin{cases} \langle \bar{u}u \rangle = \langle \bar{d}d \rangle = \langle \bar{s}s \rangle = G \equiv \langle \bar{q}q \rangle_0 \\ \langle \bar{d}\gamma_5 u + \text{h.c.} \rangle = \langle \bar{s}\gamma_5 u + \text{h.c.} \rangle = 0 \\ n_I = n_S = 0 \end{cases} \quad (22)$$

2. **Pion condensation phase**,  $\mu_I > m_\pi$  and  $\mu_S < \left(-m_\pi^2 + \sqrt{(m_\pi^2 - \mu_I^2)^2 + 4m_K^2\mu_I^2}\right) / 2\mu_I$ :

$$\begin{cases} \langle \bar{u}u \rangle = \langle \bar{d}d \rangle = G \cos \alpha = \langle \bar{q}q \rangle_0 m_\pi^2 / \mu_I^2 \\ \langle \bar{s}s \rangle = G = \langle \bar{q}q \rangle_0 \\ \langle \bar{d}\gamma_5 u + \text{h.c.} \rangle = G \sin \alpha = \langle \bar{q}q \rangle_0 \sqrt{1 - m_\pi^4 / \mu_I^4} \\ \langle \bar{s}\gamma_5 u + \text{h.c.} \rangle = 0 \\ n_I = F^2 \mu_I (1 - m_\pi^4 / \mu_I^4) \\ n_S = 0 \end{cases} \quad (23)$$

3. **Kaon condensation phase**,  $\mu_S > m_K - \mu_I / 2$  and  $\mu_S > \left(-m_\pi^2 + \sqrt{(m_\pi^2 - \mu_I^2)^2 + 4m_K^2\mu_I^2}\right) / 2\mu_I$ :

$$\begin{cases} \langle \bar{u}u \rangle = \langle \bar{s}s \rangle = G \cos \alpha = \langle \bar{q}q \rangle_0 m_K^2 / (\frac{1}{2}\mu_I^2 + \mu_S)^2 \\ \langle \bar{d}d \rangle = G = \langle \bar{q}q \rangle_0 \\ \langle \bar{d}\gamma_5 u + \text{h.c.} \rangle = 0 \\ \langle \bar{s}\gamma_5 u + \text{h.c.} \rangle = G \sin \alpha = \langle \bar{q}q \rangle_0 \sqrt{1 - m_K^4 / (\frac{1}{2}\mu_I + \mu_S)^4} \\ n_I = \frac{1}{2} F^2 (\frac{1}{2}\mu_I + \mu_S) \left(1 - m_K^4 / (\frac{1}{2}\mu_I + \mu_S)^4\right) \\ n_S = F^2 (\frac{1}{2}\mu_I + \mu_S) \left(1 - m_K^4 / (\frac{1}{2}\mu_I + \mu_S)^4\right). \end{cases} \quad (24)$$

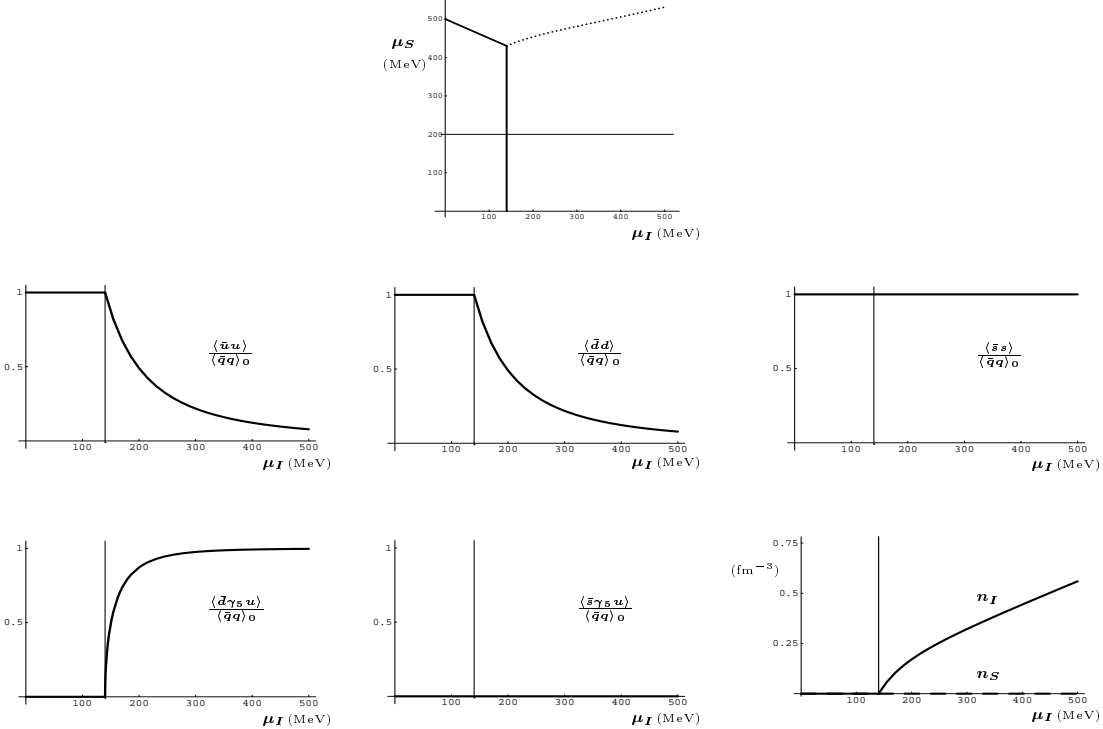


Figure 2: The figure on top is the phase diagram in the first quadrant of the  $(\mu_I, \mu_S)$ -plane. The light solid horizontal line corresponds to  $\mu_S = 200\text{MeV}$ , the value we use throughout the other figures depicted underneath. In these last six figures, the critical value of  $\mu_I$  at the second order phase transition is depicted by a solid vertical line. The different condensates are shown in the next five figures. The isospin density (solid curve) and the strangeness density (dashed curve) are shown together in the last figure.

The isospin and strangeness densities in the superfluid phases just above the second order phase transition curves can be reproduced within a semi-classical analysis of a dilute Bose gas in the Bose-Einstein condensation phase [8]. In the kaon superfluid phase, the strangeness density is naturally found to be twice bigger than the isospin density, since a kaon carries twice more strangeness than isospin.

The different condensates and charge densities as a function of  $\mu_I$  and for a constant  $\mu_S$  are depicted in Fig. 2, for  $\mu_S = 200\text{MeV}$ , and in Fig. 3, for  $\mu_S = 460\text{MeV}$ . In the first case we encounter only two phases as  $\mu_I$  changes, whereas in the second case we encounter the three different phases found above as  $\mu_I$  changes. As expected, the condensates and charge densities are continuous across the second order phase transition and discontinuous across the first order one. The different phases and the nature of the different phase transitions are clearly distinguished by the observables we study.

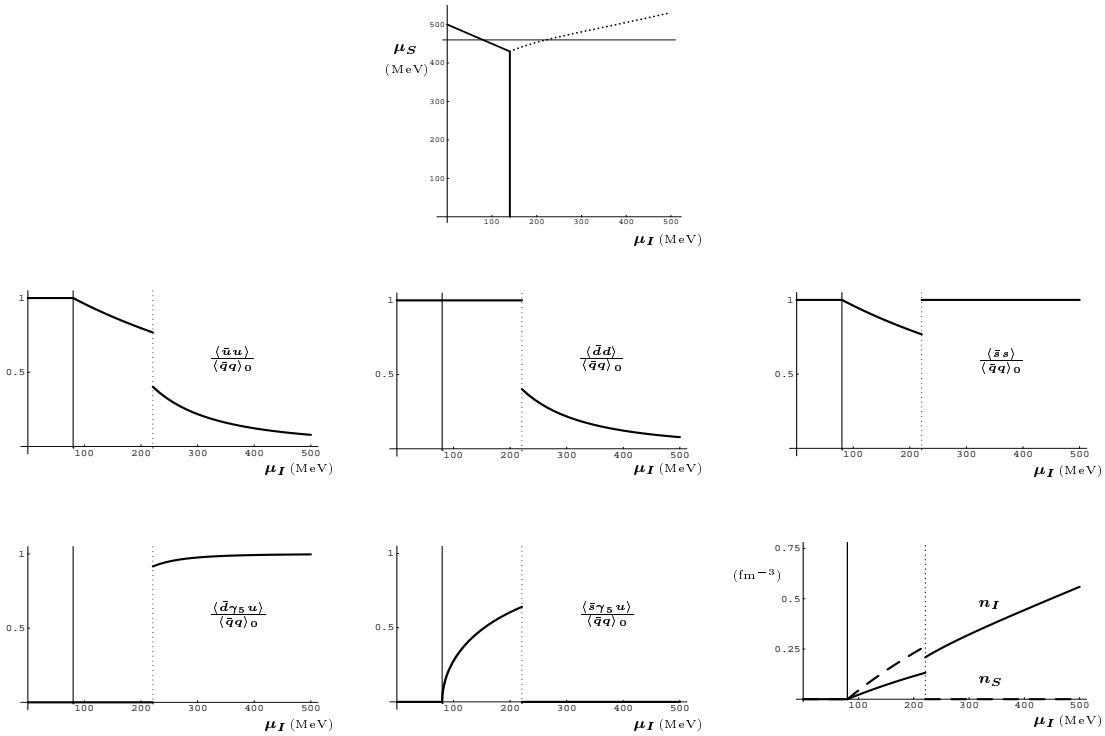


Figure 3: The figure on top is the phase diagram in the first quadrant of the  $(\mu_I, \mu_S)$ -plane. The light solid horizontal line corresponds to  $\mu_S = 460\text{MeV}$ , the value we use throughout the other figures depicted underneath. In these last six figures, the critical value of  $\mu_I$  at the second order phase transition is depicted by a solid vertical line, and the critical value of  $\mu_I$  at the first order phase transition is depicted by a dotted vertical line. The different condensates are shown in the next five figures. The isospin density (solid curve) and the strangeness density (dashed curve) are shown together in the last figure. The difference between the second and first order phase transitions are very clearly seen in these observables.

## 5 Curvatures and mass spectrum

In this section we will prove that  $\bar{\Sigma}$  given by (9,19,20,21) is indeed a local maximum of the static part of the effective Lagrangian. We compute the masses of the different excitations in the three



phases. In order to obtain these masses, we have to expand the whole effective Lagrangian up to second order in the Goldstone fields. The general form of the effective Lagrangian reads

$$\begin{aligned} \mathcal{L}_{\text{eff}} = & -\frac{F^2}{4}\text{Tr}[B, \bar{\Sigma}][B, \bar{\Sigma}^\dagger] + \frac{1}{2}G\text{Tr}\mathcal{M}(\bar{\Sigma} + \bar{\Sigma}^\dagger) \\ & + \frac{F^2}{4}\text{Tr}\partial_\nu\Sigma\partial_\nu\Sigma^\dagger + i\frac{F^2}{2}\text{Tr}B[\Sigma^\dagger, \partial_0\Sigma]. \end{aligned} \quad (25)$$

The fourth term in (25) may involve a term quadratic in the Goldstone fields (6). In the superfluid phases, the original Goldstone fields are mixed [8]. Since the usual Goldstone manifold changes as the normal phase is left, the original octet of Goldstone bosons is not an appropriate set of coordinates for the new Goldstone manifold. We will denote these new appropriate fields by a “tilde”. We choose them so that the kinetic term in the Lagrangian is canonical. Furthermore, the linear derivative term in (25) mixes these new fields. Therefore the mass spectrum is not directly given by the curvatures of the static part of the Lagrangian at the maximum. When  $n$ -fields are mixed, the inverse propagator that appears in the effective Lagrangian is a  $n \times n$  matrix, and the masses are given by the zeros of its determinant in the  $p_0^2$ -plane. A secular equation has therefore to be solved. It is a  $n$ -th order equation in  $p_0^2$  when  $n$  fields are mixed by the linear derivative term in (25). These equations can be explicitly solved, but the explicit solutions are cumbersome and rather useless expressions. Therefore we will only give which fields are mixed by the linear derivative term in (25), and solve the secular equation explicitly in the simple cases only. The labels of the different mixed states will be given according to the usual Goldstone mode they correspond to at the second order phase transition with the normal phase. We study each phase separately, and summarize our results for the mass spectrum in a few figures.

## 5.1 Normal phase

For  $\mu_I < m_\pi$  and  $\mu_S < m_K - \frac{1}{2}\mu_I$ , with the Goldstone fields defined in (6), we find that there is no mixing induced by the linear derivative term in the quadratic part of the effective Lagrangian. The various masses read

$$\begin{aligned} m_{\pi^0} &= m_\pi \\ m_{\eta^0} &= m_{\eta^0} = \sqrt{(4m_K^2 - m_\pi^2)}/3 \\ m_{\pi^+} &= m_\pi - \mu_I \\ m_{\pi^-} &= m_\pi + \mu_I \\ m_{K^+} &= m_K - \frac{1}{2}\mu_I - \mu_S \\ m_{K^-} &= m_K + \frac{1}{2}\mu_I + \mu_S \\ m_{K^0} &= m_K + \frac{1}{2}\mu_I - \mu_S \\ m_{\bar{K}^0} &= m_K - \frac{1}{2}\mu_I + \mu_S. \end{aligned} \quad (26)$$

The effect of the chemical potentials is just to shift the mass of a state by its charges times the chemical potentials:  $E \rightarrow E - I\mu_I - S\mu_S$ , where  $I$  and  $S$  are the isospin and strangeness of that state.

## 5.2 Pion condensation phase

For  $\mu_I > m_\pi$  and  $\mu_S < \left(-m_\pi^2 + \sqrt{(m_\pi^2 - \mu_I^2)^2 + 4m_K^2\mu_I^2}\right)/2\mu_I$ , we find that there is mixing between some of the fields defined in (6), namely  $(\pi^0, \eta^0, \pi^+, \pi^-)$ , and  $(K^+, K^-, K^0, \bar{K}^0)$ . We

find that the different masses are given by

$$\begin{aligned}
m_{\tilde{\pi}^0}^2 &= \mu_I^2 \\
m_{\tilde{\eta}^0}^2 &= \frac{1}{6\mu_I^2} \left( 4m_K^2 \mu_I^2 - 2m_\pi^2 \mu_I^2 + 6m_\pi^4 + 7\mu_I^4 + \left[ 48m_\pi^6 (\mu_I^2 - m_\pi^2) \right. \right. \\
&\quad \left. \left. + \mu_I^4 (4m_K^2 + \mu_I^2)^2 - 4m_\pi^4 \mu_I^2 (24m_K^2 - 43\mu_I^2) - 4m_\pi^2 \mu_I^4 (4m_K^2 + \mu_I^2) \right]^{1/2} \right) \\
m_{\tilde{\pi}^+}^2 &= 0 \\
m_{\tilde{\pi}^-}^2 &= \frac{1}{6\mu_I^2} \left( 4m_K^2 \mu_I^2 - 2m_\pi^2 \mu_I^2 + 6m_\pi^4 + 7\mu_I^4 - \left[ 48m_\pi^6 (\mu_I^2 - m_\pi^2) \right. \right. \\
&\quad \left. \left. + \mu_I^4 (4m_K^2 + \mu_I^2)^2 - 4m_\pi^4 \mu_I^2 (24m_K^2 - 43\mu_I^2) - 4m_\pi^2 \mu_I^4 (4m_K^2 + \mu_I^2) \right]^{1/2} \right),
\end{aligned} \tag{27}$$

and the masses of  $\tilde{K}^+$ ,  $\tilde{K}^-$ ,  $\tilde{K}^0$ ,  $\tilde{K}^{\tilde{0}}$  are given by the zeros on the  $E$ -plane of

$$\det \begin{pmatrix} \frac{1}{2}E^2 + s_1 & Es_2 & Es_3 & 0 \\ Es_2^\dagger & \frac{1}{2}E^2 + s_1 & 0 & Es_3 \\ Es_3^\dagger & 0 & \frac{1}{2}E^2 + s_1 & Es_4 \\ 0 & Es_3^\dagger & Es_4^\dagger & \frac{1}{2}E^2 + s_1 \end{pmatrix}, \tag{28}$$

where

$$\begin{aligned}
s_1 &= \frac{1}{2}(-m_K^2 - \frac{1}{4}\mu_I^2 + \mu_S^2 + \mu_I(\frac{1}{2}\mu_I + \mu_S) \cos \alpha) \\
s_2 &= i(\mu_S + \frac{1}{2}\mu_I \cos \alpha) \\
s_3 &= \frac{1}{2}\mu_I \sin \alpha \\
s_4 &= i(\mu_S - \frac{1}{2}\mu_I \cos \alpha),
\end{aligned} \tag{29}$$

and  $\cos \alpha = (m_\pi/\mu_I)^2$ , as given in (20).

### 5.3 Kaon condensation phase

For  $\mu_S > m_K - \mu_I/2$  and  $\mu_S > \left( -m_\pi^2 + \sqrt{(m_\pi^2 - \mu_I^2)^2 + 4m_K^2 \mu_I^2} \right) / 2\mu_I$ , we find that there is mixing between some of the fields defined in (6), namely  $(\pi^0, \eta^0, K^+, K^-)$ , and  $(\tilde{\pi}^+, \tilde{\pi}^-, \tilde{K}^0, \tilde{K}^{\tilde{0}})$ . The masses of  $\tilde{\pi}^0, \tilde{\eta}^0, \tilde{K}^+, \tilde{K}^-$  are given by the zeros in the  $E$ -plane of

$$\det \begin{pmatrix} \frac{1}{2}E^2 + t_{11} & t_{12} & 0 & 0 \\ t_{12}^\dagger & \frac{1}{2}E^2 + t_{22} & Et_{23} & 0 \\ 0 & Et_{23}^\dagger & \frac{1}{2}E^2 & Et_{34} \\ 0 & 0 & Et_{34}^\dagger & \frac{1}{2}E^2 + t_{44} \end{pmatrix}, \tag{30}$$

where

$$\begin{aligned}
t_{11} &= -\frac{1}{2\cos \alpha} m_K^2 \\
t_{12} &= \frac{1}{2\sqrt{3}} (m_K^2 - m_\pi^2) \\
t_{22} &= -\frac{1}{6} (2m_\pi^2 + m_K^2 \cos \alpha) \\
t_{23} &= -\frac{1}{\sqrt{3}} (\frac{1}{2}\mu_I + \mu_S) \sin \alpha \\
t_{34} &= -i(\frac{1}{2}\mu_I + \mu_S) \cos \alpha \\
t_{44} &= \frac{1}{2} (-m_K^2 \cos \alpha + (\frac{1}{2}m\mu_I + \mu_S)^2 \cos 2\alpha),
\end{aligned} \tag{31}$$

and  $\cos \alpha = (m_K/(\frac{1}{2}\mu_I + \mu_S))^2$ , as given in (21). One of the modes, the  $\tilde{K}^+$ , is massless. The masses of  $\tilde{\pi}^+, \tilde{\pi}^-, \tilde{K}^0, \tilde{K}^{\tilde{0}}$  are given by the zeros on the  $E$ -plane of

$$\det \begin{pmatrix} \frac{1}{2}E^2 + u_1 & Eu_2 & Eu_3 & 0 \\ Eu_2^\dagger & \frac{1}{2}E^2 + u_1 & 0 & -Eu_3 \\ Eu_3^\dagger & 0 & \frac{1}{2}E^2 + u_4 & Eu_5 \\ 0 & -Eu_3^\dagger & Eu_5^\dagger & \frac{1}{2}E^2 + u_4 \end{pmatrix}, \tag{32}$$

where

$$\begin{aligned}
u_1 &= \frac{1}{4}(-2m_\pi^2 + \mu_I^2 - 2\mu_I\mu_S + 2\mu_I(\frac{1}{2}\mu_I + \mu_S) \cos \alpha) \\
u_2 &= \frac{i}{4}(3\mu_I - 2\mu_S + 2(\frac{1}{2}\mu_I + \mu_S) \cos \alpha) \\
u_3 &= \frac{1}{2}(\frac{1}{2}\mu_I + \mu_S) \sin \alpha \\
u_4 &= \frac{1}{8}(-4m_K^2 + 2\mu_I^2 - 4\mu_I\mu_S - \mu_I^2 \cos \alpha + 4\mu_S^2 \cos \alpha) \\
u_5 &= \frac{i}{4}(-3\mu_I + 2\mu_S + 2(\frac{1}{2}\mu_I + \mu_S) \cos \alpha),
\end{aligned} \tag{33}$$

and  $\cos \alpha = (m_K / (\frac{1}{2}\mu_I + \mu_S))^2$ , as given in (21).

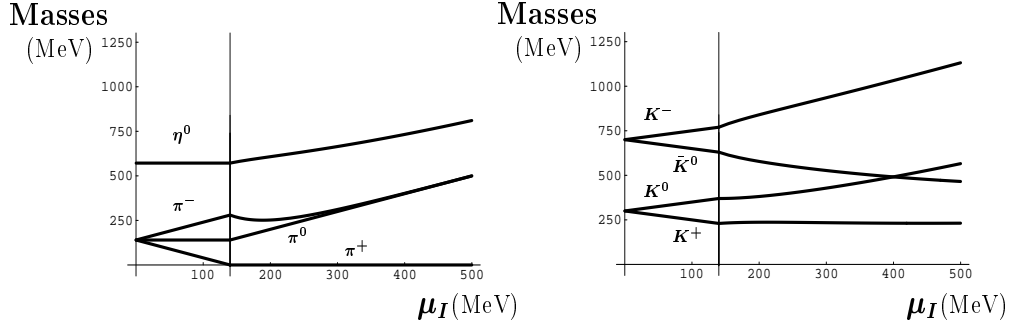


Figure 4: The masses of the eight pseudo-Goldstone bosons are shown here as a function of  $\mu_I$  for  $\mu_S = 200\text{MeV}$ . In these two figures, the critical value of  $\mu_I$  at the second order phase transition is depicted by a solid vertical line.

The spectrum is depicted as a function of  $\mu_I$  for  $\mu_S = 200\text{MeV}$  in Fig. 4, and for  $\mu_S = 460\text{MeV}$  in Fig. 5, the corresponding condensates and densities are given in Fig. 2, and in Fig. 3, respectively. The masses are continuous across the second order phase transition lines, as they should, and they are in general discontinuous across the first order phase transition curves, as they might. In each superfluid phase there is one single massless Goldstone mode. The  $SU_V(3) \times U_V(1)$  symmetry that leaves the quark-antiquark condensate invariant is further broken by the new condensates in the superfluid phases:  $U_I(1)$  symmetry is broken by the pion condensate, and  $U_S(1)$  is broken by the kaon condensate.

## 6 Conclusions

In this article we have explored part of the phase diagram of QCD at non-zero quark chemical potentials and zero temperature. We have used a low-energy effective theory based on the symmetries of the QCD partition function, Chiral Perturbation Theory. The quark chemical potentials have been introduced into the effective Lagrangian as a usual vector external source via a flavor gauge symmetry. Because we only kept the octet of the Goldstone bosons as relevant degrees of freedom, which is only justified for small enough chemical potentials, our analysis is intrinsically limited to the domain  $|\mu_u| < 300\text{MeV}$ ,  $|\mu_d| < 300\text{MeV}$ , and  $|\mu_s| < 550\text{MeV}$ . But this *whole* domain can be reached within Chiral Perturbation Theory.

We have found a non-trivial phase diagram. There are three distinct phases: a normal phase, a pion superfluid phase, and a kaon superfluid phase. The two superfluid phases are separated

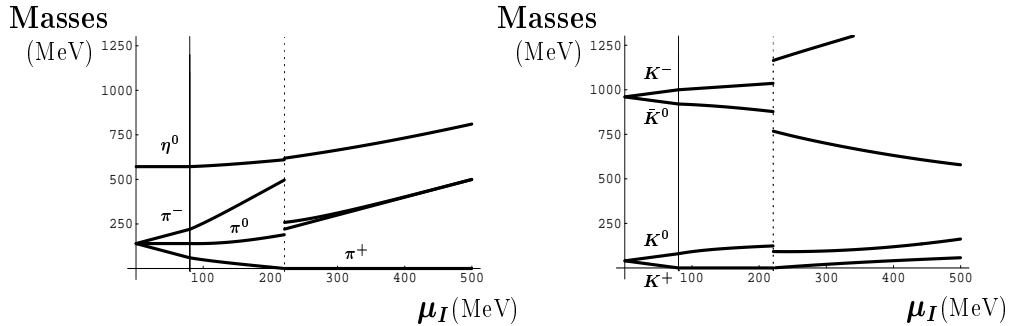


Figure 5: The masses of the eight pseudo-Goldstone bosons are shown here as a function of  $\mu_I$  for  $\mu_S = 460\text{MeV}$ . In these two figures, the critical value of  $\mu_I$  at the second order phase transition is depicted by a solid vertical line, and the critical value of  $\mu_I$  at the first order phase transition is depicted by a dotted vertical line.

by a first order phase transition curve, whereas each of them is separated from the normal phase by a second order phase transition curve. The observables that we have analyzed show a typical behavior for such a phase diagram. The behavior of the different condensates at the second order phase transitions is very similar to what has been found in QCD-like theories [8, 9]. The number densities just above the second order phase transition curves can be understood from a dilute gas approximation [8]. The excitation spectrum in the normal phase is trivial, and there is one massless mode in each superfluid phase that is due to further spontaneous symmetry breaking by the unusual condensates, similar to what as been observed in QCD-like theories [7, 8, 9].

Our study extends the analysis of QCD at non-zero isospin chemical potential done by Son and Stephanov [14]. We recover all their results on the pion condensate, the isospin number density and the mass spectrum for  $|\mu_S| < m_K - m_\pi/2 = 430\text{MeV}$ , where kaon condensation can become energetically more favorable, depending on  $\mu_I$  (cf. Fig.1, 2, 4).

Finally, at low energy and within the effective theory approach we have used, it would be interesting to study matter that is not only made out of quarks and gluons, but also electrons and neutrinos. The inclusion of the electro-magnetic interaction and of the weak interaction into Chiral Perturbation Theory has already been achieved in the vacuum [18], and its generalization to non-zero quark chemical potential seems to be rather straightforward. The effective theory technique we have used in this article is therefore very well suited to study more general problems of this kind.

## Acknowledgments

G. Baym, M. Stephanov and J. Verbaarschot are acknowledged for useful discussions. J.B.K. is supported in part by the National Science Foundation, NSF-PHY96-05199. D.T. is supported in part by “Holderbank”-Stiftung.

## References

- [1] D. Bailin and A. Love, Phys. Rept. **107**, 325 (1984).
- [2] M. Alford, K. Rajagopal and F. Wilczek, Phys. Lett. **B422**, 247 (1998); Nucl. Phys. **B537**, 443 (1999).
- [3] R. Rapp, T. Schafer, E. V. Shuryak and M. Velkovsky, Phys. Rev. Lett. **81**, 53 (1998); Annals Phys. **280**, 35 (2000).
- [4] K. Rajagopal and F. Wilczek, hep-ph/0011333.
- [5] A. V. Smilga, Phys. Rept. **291**, 1 (1997); and references therein.
- [6] S. Chandrasekharan and U. Wiese, Phys. Rev. Lett. **83**, 3116 (1999); M. Alford, S. Chandrasekharan, J. Cox and U. J. Wiese, hep-lat/0101012.
- [7] J. B. Kogut, M. A. Stephanov and D. Toublan, Phys. Lett. **B464**, 183 (1999).
- [8] J. B. Kogut, M. A. Stephanov, D. Toublan, J. J. Verbaarschot and A. Zhitnitsky, Nucl. Phys. **B582**, 477 (2000).
- [9] K. Splittorff, D. T. Son and M. A. Stephanov, hep-ph/0012274.
- [10] S. Hands, I. Montvay, S. Morrison, M. Oevers, L. Scorzato and J. Skullerud, Eur. Phys. J. C **17**, 285 (2000) [hep-lat/0006018].
- [11] R. Aloisio, A. Galante, V. Azcoiti, G. Di Carlo and A. F. Grillo, hep-lat/0007018; R. Aloisio, V. Azcoiti, G. Di Carlo, A. Galante and A. F. Grillo, Phys. Lett. B **493**, 189 (2000)
- [12] Y. Liu, O. Miyamura, A. Nakamura and T. Takaishi, hep-lat/0009009.
- [13] S. J. Hands, B. Kogut, S. E. Morrison and D. K. Sinclair, Nucl. Phys. Proc. Suppl. **94**, 457 (2001).
- [14] D. T. Son and M. A. Stephanov, hep-ph/0005225; hep-ph/0011365.
- [15] S. Weinberg, Physica **A96**, 327 (1979).
- [16] J. Gasser and H. Leutwyler, Annals Phys. **158**, 142 (1984); Nucl. Phys. **B250**, 465 (1985).
- [17] A. Migdal, Zh. Eksp. Teor. Fiz. 61 (1971) 2210 [Sov. Phys. JETP 36 (1973) 1052]; R.F. Sawyer, Phys. Rev. Lett. 29 (1972) 382; D.J. Scalapino, Phys. Rev. Lett. 29 (1972) 386; G. Baym, Phys. Rev. Lett. 30 (1973) 1340; D.B. Kaplan and A.E. Nelson, Phys. Lett. B175 (1986) 57; H.D. Politzer and M.B. Wise, Phys. Lett. B273 (1991) 156; C.-H. Lee, G.E. Brown, D.-P. Min and M. Rho, Nucl. Phys. A585 (1995) 401.
- [18] A. Pich, in *Les Houches Summer School in Theoretical Physics, Session 68: Probing the Standard Model of Particle Interactions*, R. Gupta, A. Morel, E. de Rafael and F. David eds, North-Holland (1999), hep-ph/9806303; and references therein.